Hindawi
Computational Intelligence and Neuroscience
Volume 2022, Article ID 2728866, 12 pages
https://doi.org/10.1155/2022/2728866

Research Article

Multithreshold Segmentation and Machine Learning Based Approach to Differentiate COVID-19 from Viral Pneumonia

Shaik Mahaboob Basha,[1,2] **Aloísio Vieira Lira Neto**,[2] **Samah Alshathri**,[3] **Mohamed Abd Elaziz**,[4] **Shaik Hashmitha Mohisin**,[5] **and Victor Hugo C. De Albuquerque**[6]

[1]*Department of Electronics and Communication Engineering, Geethanjali Institute of Science and Technology, Nellore, India*
[2]*Graduation Program in Telecommunication Engineering, Federal Institute of Ceará, Fortaleza, CE, Brazil*
[3]*Department of Information Technology, College of Computer and Information Sciences, Princess Nourah bint Abdulrahman University, P.O. Box 84428, Riyadh 11671, Saudi Arabia*
[4]*Faculty of Computer Science and Engineering, Galala University, Suez 435611, Egypt*
[5]*Department of Electrical and Electronics Engineering, National Institute of Technology Calicut, Kozhikode 673601, India*
[6]*Department of Teleinformatics Engineering, Federal University of Ceará, Fortaleza, CE, Brazil*

Correspondence should be addressed to Shaik Mahaboob Basha; mohisin7@yahoo.co.in, Samah Alshathri; sealshathry@pnu.edu.sa, and Mohamed Abd Elaziz; abd_el_aziz_m@yahoo.com

Received 30 April 2022; Revised 13 June 2022; Accepted 5 July 2022; Published 20 August 2022

Academic Editor: Abdul Rehman Javed

Coronavirus disease (COVID-19) has created an unprecedented devastation and the loss of millions of lives globally. Contagious nature and fatalities invariably pose challenges to physicians and healthcare support systems. Clinical diagnostic evaluation using reverse transcription-polymerase chain reaction and other approaches are currently in use. The Chest X-ray (CXR) and CT images were effectively utilized in screening purposes that could provide relevant data on localized regions affected by the infection. A step towards automated screening and diagnosis using CXR and CT could be of considerable importance in these turbulent times. The main objective is to probe a simple threshold-based segmentation approach to identify possible infection regions in CXR images and investigate intensity-based, wavelet transform (WT)-based, and Laws based texture features with statistical measures. Further feature selection strategy using Random Forest (RF) then selected features used to create Machine Learning (ML) representation with Support Vector Machine (SVM) and a Random Forest (RF) to make different COVID-19 from viral pneumonia (VP). The results obtained clearly indicate that the intensity and WT-based features vary in the two pathologies that are better differentiated with the combined features trained using SVM and RF classifiers. Classifier performance measures like an Area Under the Curve (AUC) of 0.97 and by and large classification accuracy of 0.9 using the RF model clearly indicate that the methodology implemented is useful in characterizing COVID-19 and Viral Pneumonia.

1. Introduction

The extremely infectious nature of coronavirus disease (COVID-19), which has been declared a pandemic, has paved the way for a phenomenally high infection rate, leading to overburdened healthcare systems globally [1, 2]. COVID-19 pneumonia has an irreversible tendency to progress into respiratory system collapse, multiple organ dysfunction, and even fatality. Chest X-ray (CXR) radiography is used predominantly for screening, assessment, and diagnosing different categories of pneumonia and proved to be cost effective[3–6]. Researchers concluded that CXR proved to be useful in disease prognostic studies [7]. With the aid of certain CXR-based characteristic features, it has become possible for radiologists to diagnose viral pneumonia (VP) [3, 8].

Table 1: Some of the recent works are related to our proposed work.

S. no	Author & year	Technique used	Outcome
1	Bhattacharya S et al., 2021	Deep learning techniques used for COVID-19 medical image processing.	Controlling the outbreak and controlling the crisis.
2	KIran Saleem et al. 2022	Situation-aware along with belief-desire-intention intelligent mechanisms.	Mapping the system design using NetLogo.
3	M. Manoj et al. 2020	Blockchain techniques utilized for devolution and immutability of COVID-19 data.	Deals with economic crisis in post-COVID-19.
4	Asnaoui et.al., 2021	Assessment of deep CNN in routine binary categorization of pneumonia images by VGG16, VGG19 etc.,	Improving the accuracy in diagnosis.
5	Oh, Yujin et al. 2020	Patch-based CNN in combination with artificial intelligence.	Saliency maps for COVID-19 diagnosis using CXR images.
6	Asif Iqbal Khan et al. 2020	Xception architecture on ImageNet dataset equipped by considering king COVID-19 and viral pneumonia with CXR images.	Improving the accuracy in diagnosis with large training data.
7	Hemdan et al.2020	Deep learning COVIDX-Net frame work in radiology of CXR images of COVID-19.	COVID-19 diagnosis

Some of the CXR characteristics pertaining to COVID-19 pneumonia encompass consolidation, ground glass opacity and spread across peripheral and lower zones with bilateral involvement [6]. CXR was employed for triage to determine the precedence of patients to be treated [9]. Currently, machine learning (ML) plays a predominantly instrumental part in addressing several diagnostic challenges, including detection of breast cancer, brain tumour detection, and lung cancer, [10, 11]. The relentless evolution and outreach of deep learning (DL) has further enhanced and led to a wider usability of artificial intelligence in medical informatics, including CXR processing [9]. Differentiating normal CXR and different categories of cases of pneumonia, including COVID-19, has been attempted with the aid of Alex Net-based DL [11, 12]. Handcrafted feature extraction using different transforms and texture computations in conjunction with ML-based models has also been investigated to serve the purpose of providing aid in CXR-based screening for COVID-19 [13, 14]. There exist several approaches to extract features from images, including histogram based, texture based, transform based, and key point based. Based on the features of the image, they need to be extracted which further need scientific evaluation. The texture-based feature extraction adopts several techniques to compute the texture, to name a few grey co-occurrences matrix-based computation, Laws texture computation, fractal-based models, and Gabor filter based texture extraction [15, 16]. Essentially texture is the information that reveals how frequently the intensity patterns available in a given image manifests repeatedly. Texture provides very useful insight into the inherent characteristics of the image that could be used for image analysis [17]. It has proven its usability in object recognition, segmentation, and content-based image retrieval in a broad range of image processing applications including medical images, remote sensing, and multimedia images [18]. Pixel intensity value and texture play a key role in visual recognition of the subtle patterns in an image; the ability of the human visual recognition system to process this stimulus is the primary skill to interact efficiently with the surrounding environment [19]. A comprehensive literature survey was carried out for the problem statement and was listed in Table 1.

Processing and reproducing these human features using computer systems has been a much-researched topic in the current era [20, 21]. Laws texture features were extensively applied to extract the texture features and further build machine learning models to categorize a different set of images including medical images such as Ultrasound images, microscopic images, CT, and MRI based images to cater for various pathologies [22, 23]. Microscopic biopsy images were used to extract texture features using Laws, GLCM, Wavelet, and Tamura's features with an impression that these features were easily interpretable and further with the aid of the ML model classified as cancerous and noncancerous [24]. Histogram of gradient (HOG), local binary patterns (LBP), Haralick, and other features were explored, and for each category of features, an individual ML model is constructed to explore the usability of texture features to categorize COVID-19 images from normal [25, 26]. The thresholded version of LBP texture features with the ML model and simple intensity-based statistics were explored to categorize different staining patterns of immune-fluorescence (IIF) microscopic images [27, 28]. Effective feature extraction does need efficient preprocessing of input images and several approaches were attempted with emphasis on preserving edge information along with conventional preprocessing techniques. Kumar et al. evolved the analysis of stages implicated in the augmentation of microscopic images. The segmentation of background cells and features extraction was considered in their work which ends in classification [29].

The Group Search Optimization Algorithm depicted for optimization to optimize the sequences obtained from the mining process was discussed by Lakshmanna and Khare [30]. The technique concatenating spatial pyramid Zernike moments based shape features and Law's texture derived for capturing the macro and microdetails of each facial expression [31].

Dourado et al. deduced an approach and is validated among three medical databases. The cerebral vascular accident images, lung nodule image data set, and skin image data set for stroke type, malignant, and melanocytic lesions classifications, respectively, [32]. Krishnamurthy et al. proposed an algorithm for liver diagnosis using ultrasound images. Usage of

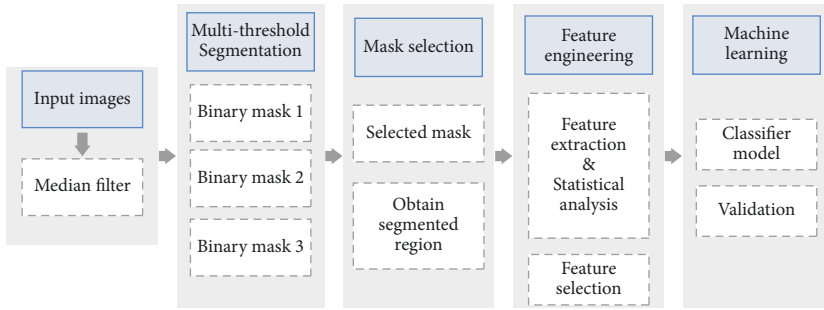

Figure 1: Block diagram of the implementation.

segmentation is another important feature in this work. It creates a space for researchers to pave a path for the interesting challenge at each phase from segmentation towards classification [33]. Ohata et al. derived a technique for automatic detection of COVID-19 infection using CXR images through transfer learning [34]. Hasoon et al derived a two classification model to detect the abnormal case of COVID-19. The preprocessing is applied for image thresholding and noise removal in this technique. The morphological operation, ROI detection, and feature extraction are salient features of this work [35].

Susaiyah et al. implemented image segmentation by means of multilevel Otsu thresholding. This was validated through using Dice's coefficient; the Jaccard index and accuracy recommend the first amongst four levels in Otsu [36]. Parvaze and Ramakrishnan considered thirteen Positive and intermediate intensity level images with homogenous, Centro mere, and Nucleolus patterns for LS based segmentation to extract objects of interest [37]. Image Denoising Technique for Ultrasound Images was deduced for structure preserving ability and efficacy [38]. An anisotropic diffusion smoothing filter is utilized to obtain a smoothing effect across the boundaries [39]. Another optimization algorithm derived from the PS algorithm implemented for the mining of sequences. The three different parameters length, weight, and RE are used for identifying frequent patterns. Ramaniharan et al. implemented a technique to analyze the shape changes. The shape based Laplace Beltrami (LB) Eigen value features. The machine learning is the optimum in this case and is highlighted in the work [40]. Bhattacharya et al. implemented a Deep learning technique in COVID-19 analysis [41]. Saleem et al. derived an approach with Situation-aware BDI Reasoning for identifying the early on symptoms of COVID-19 by means of a smart watch [42]. Basha et al. used a denoising algorithm for the accurate calculation using WNNM in ultrasound Images of COVID-19 [43, 44]. Different image compression techniques which are further useful for retrieving the data and transmission in multimedia in the post-COVID scenario [45, 46]. Gadekallu et al. contributed the procedures for near the beginning detection of Retinopathy due to diabetes. The techniques employed are PCA-Firefly based Deep Learning model. [47, 48].

Along with preprocessing, segmentation of the region of interest is necessary for designing effective strategies to delineate the tissue of interest [14, 49, 50].

After a widespread literature survey, we derived a technique made to formulate a comprehensive strategy to distinguish COVD-19 and VP with the aid of CXR by computing first-order statistical features, wavelet-based features, and laws texture features. The extracted features were subjected to feature selection using Random Forest (RF) and finally training the above features using a support vector machine (SVM) and RF classifiers. The salient features of the work is to use the fusion of statistical features, Wavelet features, and Laws texture features within the threshold region.

The main contributions are as follows:

(i) Utilization of the multithreshold approach to segment and thereby extract the texture features

(ii) Visualization of the feature maps

(iii) Investigating the handcrafted features that could identify the desired pathology

Thus, the novelty in our work is the utilization of the most significant features to construct the machine learning model.

2. Methodology

The block diagram representing the step-by-step computation is shown in Figure 1. The input CXR images considered herein were derived from the Kaggle repository [2, 10]. The goal of this study was to scrutinize the variations in CXR images pertaining to COVID-19 and VP; hence, only these two categories were taken up for a thorough examination. In the dataset used herein, there were 3617 COVID-19 images and 1345 VP images. The input images of both categories were first converted into greyscale images. Next, the images were filtered using a median filter with a mask size of 3×3 to eliminate spurious intensities and preserve the edge information. Validation of the filtering approach and comparison with other methods were not attempted herein. Filtered images were subjected to multithreshold-based Otsu segmentation [12]. Three segmented masks were obtained in this process and the mask with the highest mean intensities from CXR was selected for further analysis. We hypothesise that the highest mean intensity mask might represent the region of interest (ROI), which includes COVID-19 as well as VP. The segmented ROI is not validated owing to the unavailability of the reality. Eight features were computed, which included first-order statistics-based features such as mean, standard deviation, skewness, and kurtosis, bottom 5 percentile, bottom 10 percentile, top 90 percentile, and top 95 percentile from original images within

the segmented mask from the segmented ROI region in the CXR. The same 8 features were obtained from wavelet transformed images across four decompositions LL, LH, HL, and HH. Also, eight statistics features were computed from Laws texture maps within the threshold masks, thus making a feature vector of 72 features for each image. Biorthogonal wavelets are subjected to a closer study owing to their multiresolution properties [8, 51].

$$W_{\psi}(a,b) = \frac{1}{\sqrt{a}} \sum_{n} \psi^{*}\left(\frac{n-b}{a}\right). \tag{1}$$

The mathematical representation of the wavelet transform is shown in the (1), where "a" and "b" are the scale and translation parameters, respectively. The SVM based classifier model operates by minimizing the cost function and can be represented as follows:

$$\min_{w,b,\xi} J(\vec{w}, \vec{\xi}) = \frac{1}{2w^{T}w} + C\sum_{n=1}^{n} \xi_{n}. \tag{2}$$

The Random Forest based classifier model functionality is to put up a strong learner from an ensemble of learners, by partitioning the data into individual trees in the forest as shown in the equation.

$$S = \frac{1}{K} \sum_{K=1}^{K} K^{\text{th}}. \tag{3}$$

The 72 extracted features were then subjected to critical statistical analysis to measure the extent of the significance of the features. Subsequently, the features were subjected to Random Forest based feature selection to extract the most useful and viable features which were employed in building the classifier model using SVM with linear kernel and RF classifier with 60% of data retained for training and 40% of data for purpose of evaluation. The classifier models are then subjected to validation using 40% of the data. Furthermore, for validation purpose the performance measures were computed including receiver operating characteristics (ROC) from which AUC is computed [52]. The classifier performance measures were also computed adopting the measures presented as follows:

$$\begin{aligned}
\text{Accuracy} &= \frac{\text{TP} + \text{TN}}{\text{TP} + \text{TN} + \text{FP} + \text{FN}},\\
\text{Sensitivity} &= \frac{\text{TP}}{\text{TP} + \text{FN}},\\
\text{Specivity} &= \frac{\text{TN}}{\text{FP} + \text{TN}},\\
\text{Recall} &= \frac{\text{TP}}{\text{TP} + \text{FN}},\\
\text{Precision} &= \frac{\text{TP}}{\text{TP} + \text{FP}},\\
F1 - \text{score} &= 2 * \frac{\text{Precision} * \text{Recall}}{\text{Precision} + \text{Recall}}.
\end{aligned} \tag{4}$$

where TP = True Positive, TN = True Negative, FP= False Positive and FN= False Negative.

The computation is performed using Python compiler 3.6 and packages including Scikit-learn. (Algorithm 1)

3. Results

Representative CXR images of COVID-19 and VP are shown in Figure 2 along with the respective histograms and gradient images. Figures 2(a) and 2(d) depict COVID-19 and VP images, respectively, whereas (b) and (*e*) represent the respective histograms, while (c) and (*f*) depict the respective gradient images. Both pathologies demonstrate the presence of infection spread but with varying intensities and possible density of high intensities observed in COVID-19 that could also be observed from the histogram. The gradient images reveal the edge information pertaining to various anatomical structures.

The median-filtered images of the representative COVID-19 and VP along with histograms and gradient images are shown in Figure 3. Figure 3(a) and 3(d) depict COVID-19 and VP images filtered using a median filter, respectively, whereas (b) and (e) represent respective histograms, while (c) and (f) depict the respective gradient images. Marginal variation is observed after performing the filtering operation compared with the histograms in Figure 2. Gradient images seem to have augmented edge information representing sharp boundaries in both pathologies as compared to the image gradient images in Figure 2. In particular, as shown in Figure 2(f), the edge information is more pronounced.

The median-filtered image and multithreshold-based Otsu segmentation outputs are depicted in Figure 4. The median-filtered images of COVID-19 and VP are shown in (a) and (f), respectively. The three regions segmented using multithreshold-based Otsu segmentation are shown in Figures 3(b) and 3(g), respectively. The three regions are binarised according to the labels shown in Figures 3(c)–3(e) belonging to COVID-19 and (h–j) to VP, respectively.

The segmented regions representing the high mean intensities pertain to label three in both COVID-19 and VP, as represented in Figures 4(e) and 4(j), respectively, are considered for feature extraction.

The wavelet-based decomposed images and histograms of the representative COVID-19 and VP are shown in Figure 5. In Figures 5(a)–5(d) the LL, LH, HL, and HH of the COVID-19 image are depicted, and Figures 5(e)–5(h) represent the corresponding histograms. In Figures 5(i)–5(l), the LL, LH, HL, and HH of the VP image are depicted and Figures 5(m)–5(p) represent the corresponding histograms. Reasonable variations were observed in the LH, HL, and HH histograms of the COVID-19 and VP images. Especially, a higher number of positive coefficients could be observed in the LH and HH sub-bands in the COVID-19 image compared to that of the VP.

The feature maps obtained using Laws texture computation are depicted in Figure 6. Figures 6(a)–6(d) represent the Laws feature maps for the COVID-19 image, while the images Figures 6(e)–6(h) represent the maps belonging to

Input: image x
(1) Preprocess given image using a median filter
(2) Apply multi-threshold on the filtered image and get 3 masks
(3) Consider the segmented with the brightest pixel intensities
(4) Extract Wavelet features at 4 decompositions, Laws texture features, and basic statistical features
(5) Use Random Forest based feature selection for obtaining the best features
(6) Construct an ML model using SVM and RF
(7) Perform the validation using training and test data
Output: Trained ML model based prediction of Pneumonia and COVID-19

Algorithm 1

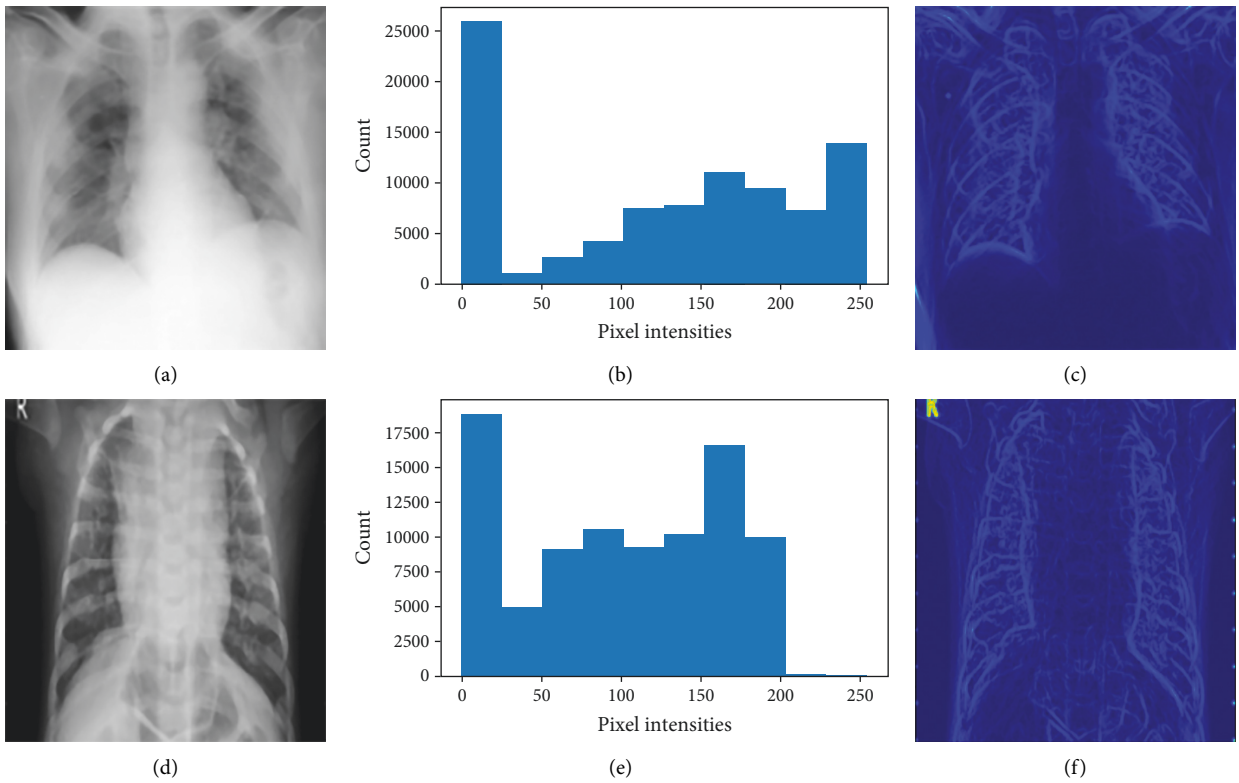

Figure 2: Representative images: (a) COVID-19, (b), (c) histogram and gradient image of (a), (d) viral pneumonia (VP), (e), (f) histogram and gradient image of (d).

the VP image. On qualitative observation, there appears to be variation in between the texture feature values of COVID-19 and VP images.

First-order, Wavelet features, and texture features were obtained directly from the segmented ROI-CXR images that were further subjected to statistical significance and to build an ML model.

The RF-based feature selection algorithm was able to pick 39 features from 72 feature vector as important features, which were further used for formulating the classifier model. The representative 8 feature values computed from HH decomposition of Wavelet transformed images were incorporated in Table 2.

The ROC plot generated using the SVM and RF classifier model for the test data is shown in Figure 7(a). The AUC of 0.97 obtained indicates that the RF classifier model can differentiate COVID-19 and VP to a large extent in comparison with the SVM. The confusion matrices for the SVM and RF are shown in Figures 7(b) and 7(c), respectively. A higher number of TPs was observed in the confusion matrix of the RF classifier, while marginally fewer FNs could be noticed in the confusion matrix of the SVM.

The performance measures obtained using the two classifier models are listed in Table 3. In comparison, increased sensitivity, F1-score, and AUC can be seen from the RF classifier.

4. Discussion

Efficient screening and diagnosis of COVID-19 methods executed with the advent of state-of-the-art image processing and ML-based approaches is needed. CXR images used by

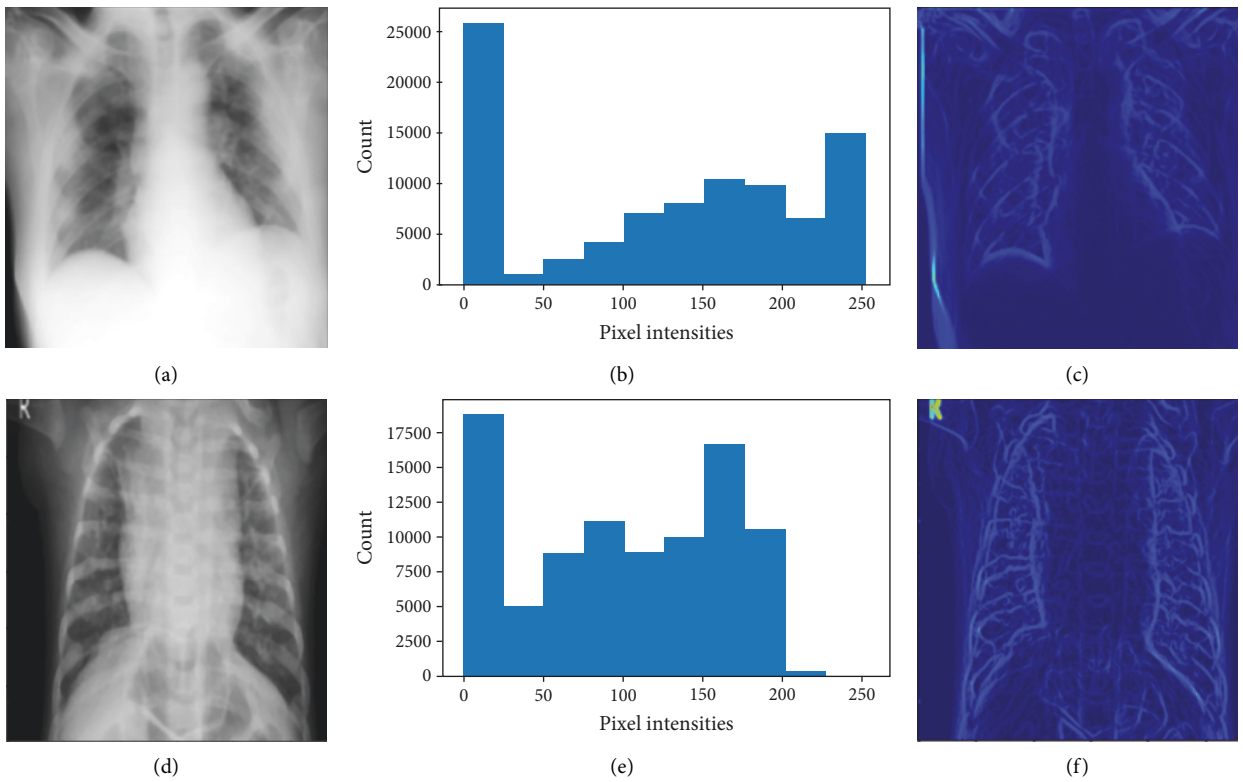

FIGURE 3: Median-filtered images: (a) COVID-19, (b), (c) histogram and gradient image of (a), (d) VP, (e), (f) histogram and gradient image of (d).

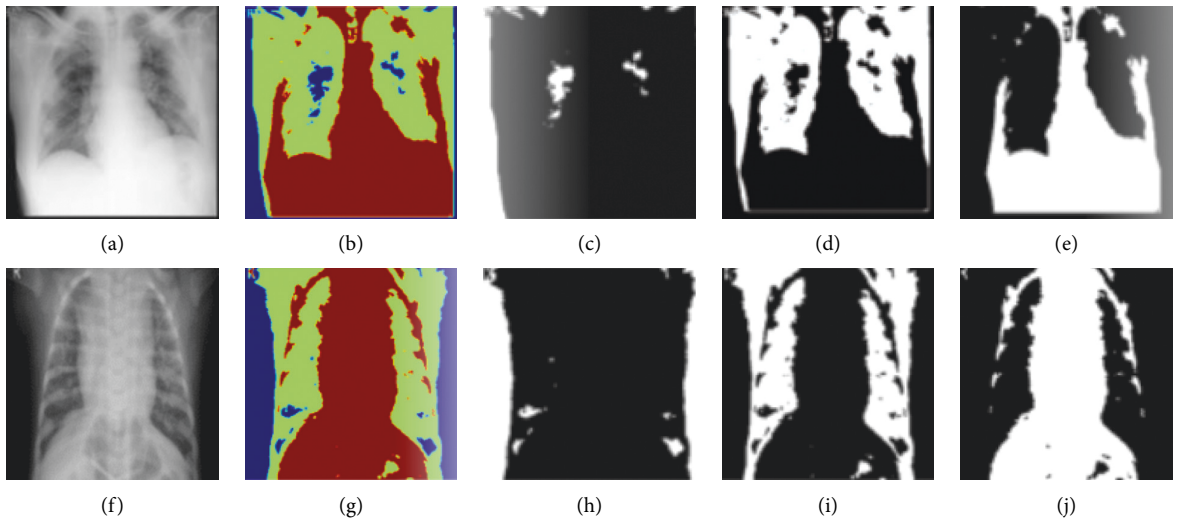

FIGURE 4: Representation of filtered and segmented images: (a) COVID-19 image (b) multi-threshold segmented labels,(c–e) three binary masks from (b), (f) VP image, (g) segmented labels, (h–j) binary masks from (g).

physicians for screening purposes provide information about the presence of the infection region and the spread of the infection. The median filter is a standard filtering process to reduce the variations in pixel intensities while preserving the edgelike information. A mask size of 3 was selected in this study to preserve the local morphology of the anatomical structures. In this work, the preprocessed images subjected to the generation of segmented masks were observed to be effective in segmenting the infection region; however, a threshold-based approach over segmentation resulting in noninfection regions was also observed. This might be due to the resemblance of the infection regions and certain anatomical regions with respect to the pixel intensities. The analysis of the histograms is deliberately attempted as the features obtained from the preprocessed images and the wavelet-decomposed images are histogram-based features.

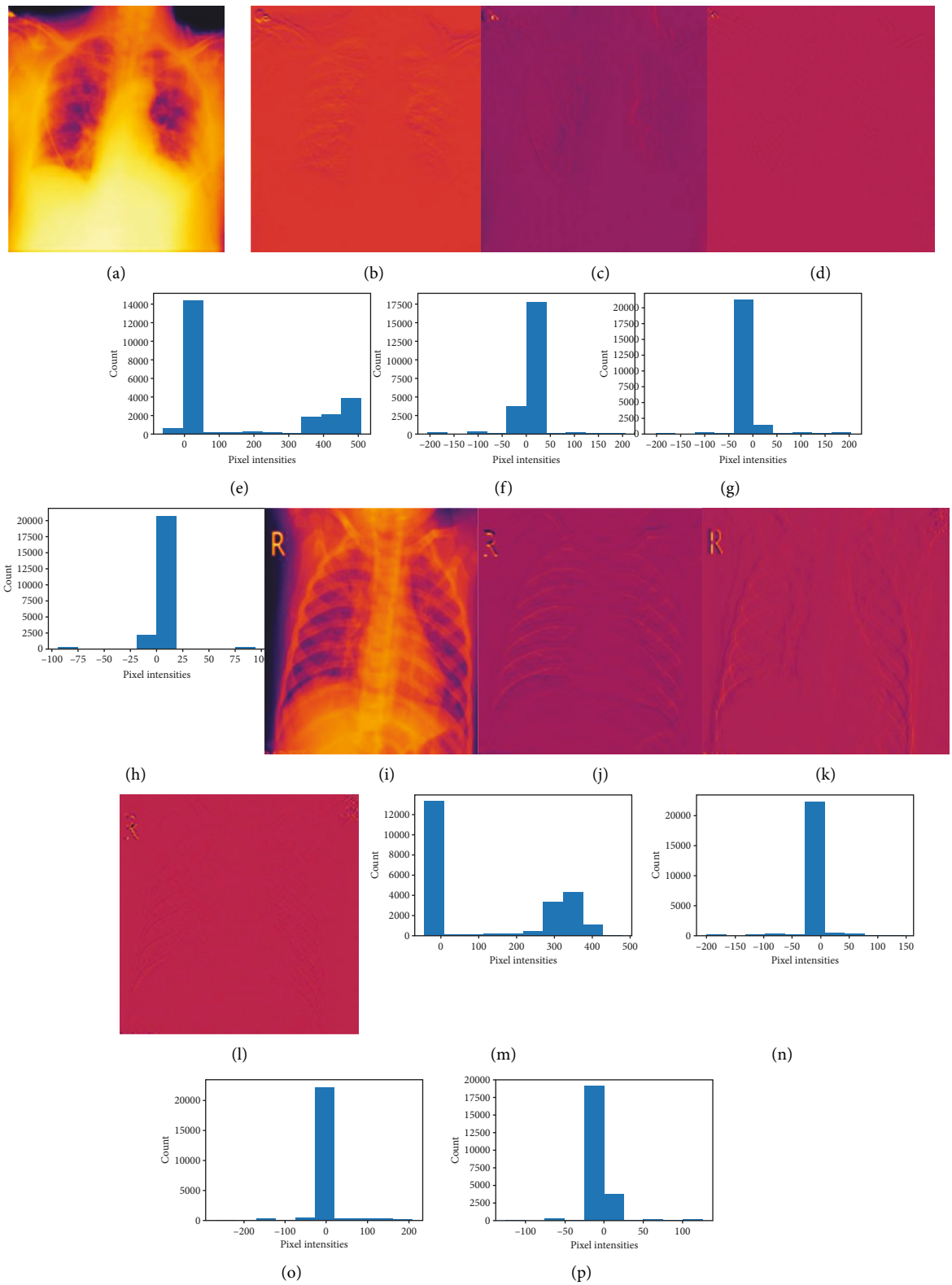

Figure 5: Wavelet decomposition images and histograms: (a–d) LL, LH, HL, and HH of COVID-19 images, (e–h) histograms of the (a–d) images, respectively, (i–l) LL, LH, HL, and HH of VP images, (m–p) histograms of the (i–l) images, respectively.

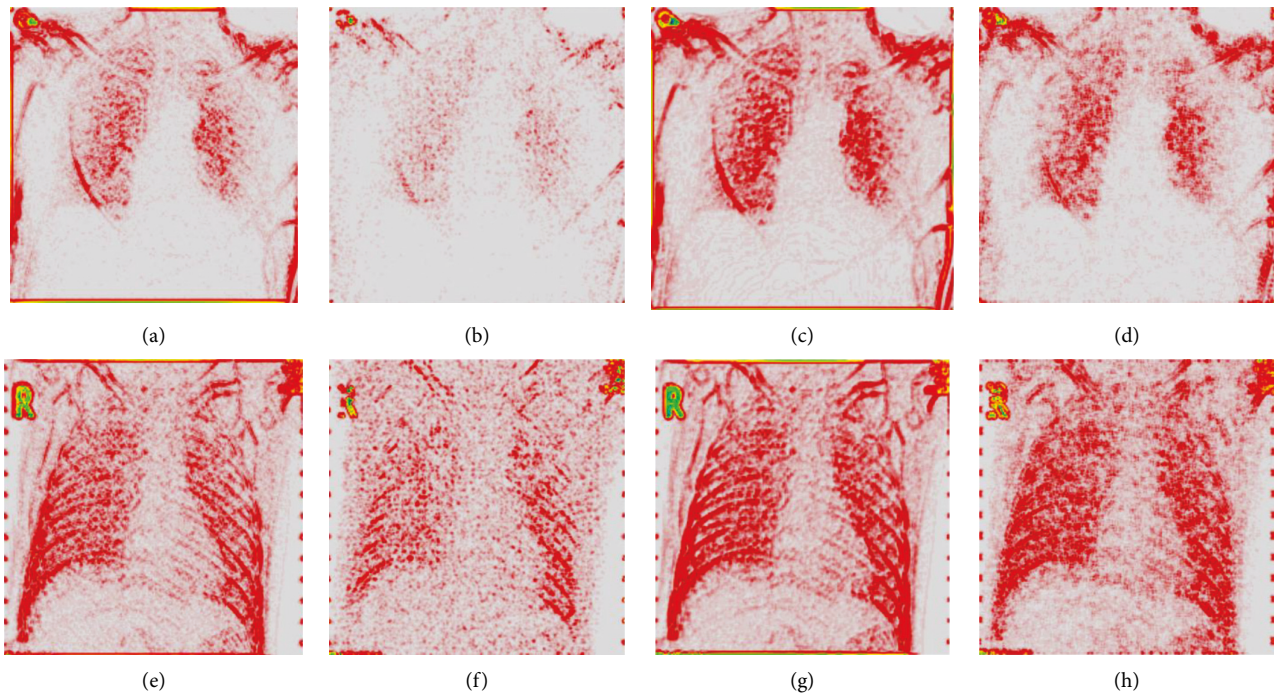

Figure 6: Laws texture feature maps (a-d) for COVID-19 image and (e-h) Viral Pneumonia image.

Table 2: Feature values for eight representative features (From wavelet decomposition at HH level).

Feature name	COVID -19 Mean ± SD	Viral pneumonia Mean ± SD	Significance value	
MnFTRWT_HH	0.00 ± 0.06	0.00 ± 0.06	0.92	Insignificant
SdFTRWT_HH	10.38 ± 1.78	10.01 ± 2.28	0.00	Significant
Skewness FTRWT_HH	−0.01 ± 0.32	−0.02 ± 0.47	0.79	Insignificant
Kurtosis FTRWT_HH	50.90 ± 18.50	69.68 ± 36.84	0.00	Significant
pr95FTRWT_HH	1.18 ± 0.36	0.92 ± 0.47	0.00	Significant
pr90FTRWT_HH	0.62 ± 0.24	0.49 ± 0.30	0.00	Significant
pr5FTRWT_HH	−1.17 ± 0.35	−0.92 ± 0.47	0.00	Significant
pr10FTRWT_HH	−0.61 ± 0.24	−0.49 ± 0.30	0.00	Significant

Hence, the morphology of the histograms was of assistance in comparative analysis. The certain intensity and WT-based feature values were observed to be more effective for differentiating COVID-19 and VP. Even though both pathologies seem to be represented by bright regions, there exist subtle variations which are picked up by most features. The differentiation of COVID-19 from VP and other CXR images has been attempted with DL and other artificial-based methods in a broad range of studies [14]. Sekeroglu B evaluated the transfer learning approach by means of pretrained networks like VGG19, and Inception ResNet [57]. Pal depicted a random forest classifier with a combination of tree classifiers. In this technique, each classifier is generated with a random vector sampled autonomously from the input vector. Each tree is used for classifying an input vector [58]. An audio signal of 4-second duration was considered for extraction of features. Finally, it was transformed onto a spectrogram and the extracted features were added and classified using ML algorithms [59]. Intracranial haemorrhage (ICH) is a serious concern with high rates of mortality. The Deep Learning technique proposed which depends on the massive amount of slice labels for training purpose [60]. Kuruoglu and Li proposed a technique using the Unscented Kalman Filter for Epidemiological Parameters for COVID-19. The non-Gaussianity and nonlinearity offers computational simplicity in this paper [61].

Rodrigues et al., feature extractors were applied to the Region of Interests (ROI) that includes nodules. The analysis of malignancy of the nodules can be studied at some stage in the classification step by incorporating ML techniques [62]. The results of the proposed technique are compared with the works cited in references [53–56]. However, these analyses were performed using entire images in the DL sense.

In this work, handcrafted features were investigated from preprocessed, Wavelet-decomposed images and Laws texture maps to understand the local inherent intensity variations. The combined features and the feature selection from the set were important to formulate the most feasible

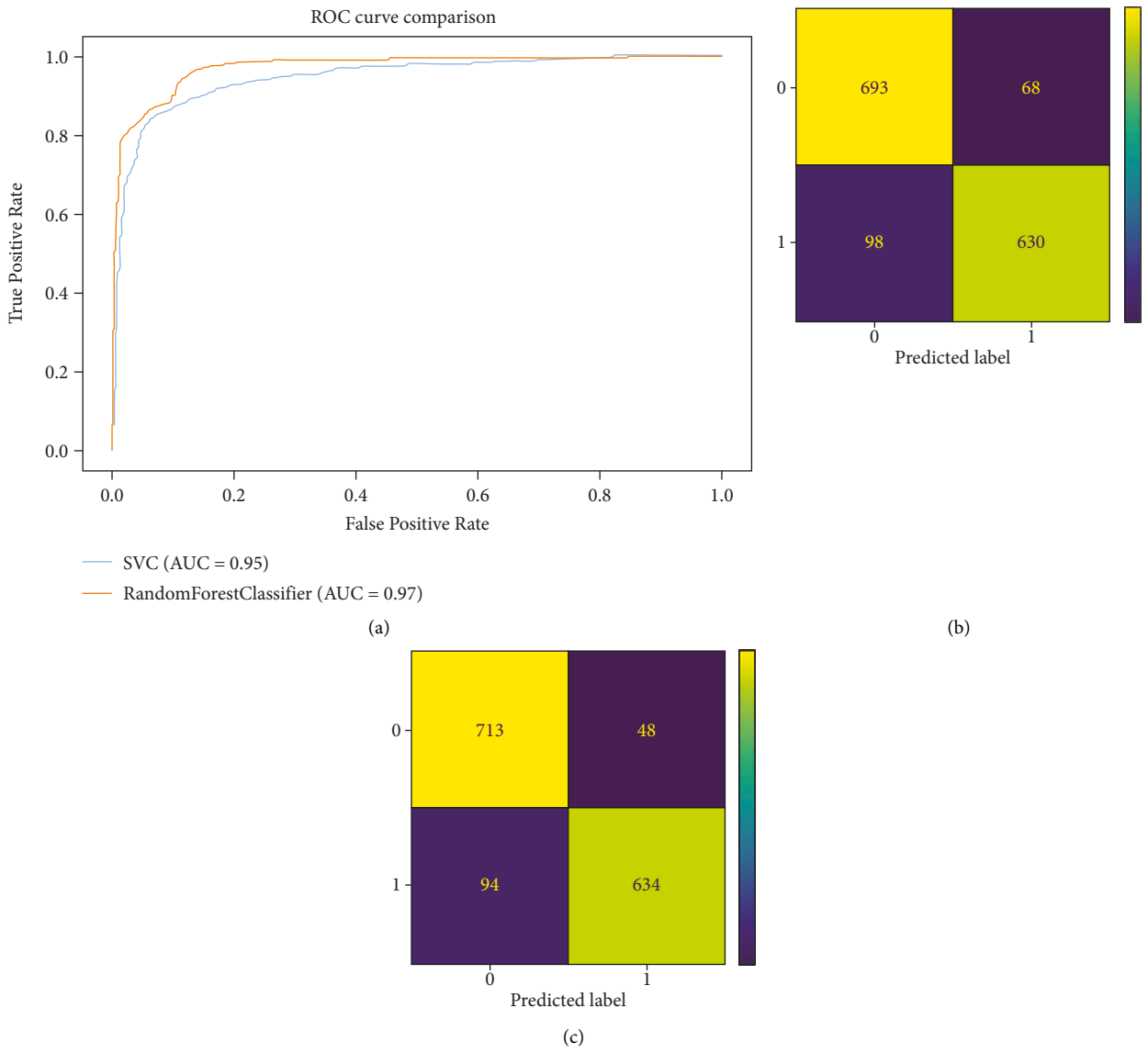

Figure 7: Classifier performance representation: (a) ROC plot for validating classifier model; (b) Confusion matrix SVM; (c) Confusion matrix RF.

Table 3: Performance measures of the classifier model.

Performance measures (%)	Support Vector Machine (SVM)	Random Forest (RF)
Accuracy	90	90
Sensitivity	78	87
Specificity	94	93
F1-score	85	90
AUC	95	97

feature vector to build the ML model. ML-based results lay further stress on the comprehensive pipeline that is necessary to address the challenges of categorising the pathologies. Even though the two ML approaches provided better results, the RF-based model outperformed the overall results. In comparison with the DL approaches, the RF model with the extracted features herein seems to have outperformed some of the studies as depicted with the accuracy parameter in Table 4. The time elapsed to compute different modules using a desktop with Intel core I5, Python 3.7, and SK-Learn ML package is represented in Table 5.

Table 4: Comparison of X-ray images studies of COVID-19.

Author	Images	Accuracy (%)	Technique used
Khalid el Asnaoui [53]	X-ray images	84	Pretrained models
YujinOh [54]	X-ray images	88.9	Pretrained models
Asif iqbal Khan [55]	X-ray images	89.5	Deep neural network
Ezz el-din Hemdan [56]	X-ray images	89	COVIDX-Net
Proposed model	X-ray images	90	SVM, Random Forest

Table 5: Time elapsed to perform different computations.

Category	Time elapsed (sec)
Feature extraction	230
Feature selection using RF	2.34
To build ML model	43

5. Conclusion

The meticulous design encompassing a comprehensive methodology utilising image analysis techniques and ML models can aid physicians and radiologists in performing efficient and accurate screening for COVID-19. Preprocessing and determining the effective region for extracting features might be essential, as comprehended from the study. In particular, the segmentation mask, even though not robust, can locate the majority of the local infection region, which might be critical in the pipeline design. The study with first-order features from preprocessed, Wavelet sub-bands and Laws texture maps integrated with the ML approach serves to discriminate the effects of COVID-19 from Viral Pneumonia for effective and exact diagnosis to mitigate the spread of the infection. Identifying the handcrafted features is a very exhaustive process and is the main limitation of the work. In the future, researchers can incorporate texture features and other forms of features including morphological features to distinguish the pathologies.

Data Availability

The data used in this paper are available from the corresponding author upon request.

Conflicts of Interest

The authors declare that they have no conflicts of interest regarding this work.

Acknowledgments

This work was funded by Princess Nourah bint Abdulrahman University Researchers Supporting under Project no. PNURSP2022R197, Princess Nourah bint Abdulrahman University, Riyadh, Saudi Arabia.

References

[1] D. Cucinotta and M. Vanelli, "WHO declares COVID-19 a pandemic," *Acta BioMedica: Atenei Parmensis*, vol. 91, no. 1, pp. 157–160, 2020.

[2] T. Rahman, T. Anas, and K. Serkan, "Exploring the effect of image enhancement techniques on COVID-19 detection using chest X-ray images," *Computers in Biology and Medicine*, vol. 132, Article ID 104319, 2021.

[3] G. Wang, X. Liu, J. Shen et al., "A deep-learning pipeline for the diagnosis and discrimination of viral, non-viral and COVID-19 pneumonia from chest X-ray images," *Nature Biomedical Engineering*, vol. 5, no. 6, pp. 509–521, 2021.

[4] C. Qin, D. Yao, Y. Shi, and Z. Song, "Computer-aided detection in chest radiography based on artificial intelligence: a survey," *Bio Medical Engineering Online*, vol. 17, no. 1, pp. 113–123, 2018.

[5] H. H. Pham, D. T. Ngo, and H. Q. Nguyenab, "Interpreting chest X-rays via CNNs that exploit disease dependencies and uncertainty labels," *Neurocomputing*, vol. 437, Article ID 19013342, 2019.

[6] M. Nishio and S. Noguchi, H. Matsuo, T. Murakami, "Automatic classification between COVID-19 pneumonia, non-COVID-19 pneumonia, and the healthy on chest X-ray image: combination of data augmentation methods," *Scientific Reports*, vol. 10, no. 1, pp. 17532–17536, 2020.

[7] A. Degerli, M. Ahishali, M. Yamac et al., "COVID-19 infection map generation and detection from chest X-ray images," *Health Information Science and Systems*, vol. 9, no. 1, pp. 15-16, 2021.

[8] K. Jaiswal, P. Tiwari, S. Kumar, D. Gupta, A. Khanna, and J. P. C. Rodrigues, "Identifying pneumonia in chest X-rays: a deep learning approach," *Measurement*, vol. 145, pp. 511–518, 2019.

[9] K. Kallianos, J. Mongan, S. Antani et al., "How far have we come? Artificial intelligence for chest radiograph interpretation," *Clinical Radiology*, vol. 74, no. 5, pp. 338–345, 2019.

[10] M. E. H. Chowdhury, T. Rahman, A. Khandakar et al., "Can AI help in screening viral and COVID-19 pneumonia?" *IEEE Access*, vol. 8, pp. 132665–132676, 2020.

[11] A. U. Ibrahim, M. Ozsoz, S. Serte, F. Al-Turjman, and P. S. Yakoi, "Pneumonia classification using deep learning from chest X-ray images during COVID-19," *Cognitive Computation*, pp. 1–13, 2021.

[12] A. Waheed, M. Goyal, D. Gupta, A. Khanna, F. Al-Turjman, and P. R. Pinheiro, "CovidGAN: data augmentation using auxiliary classifier gan for improved covid-19 detection," *IEEE Access*, vol. 8, pp. 91916–91923, 2020.

[13] L. Hussain, T. Nguyen, H. Li et al., "Machine-learning classification of texture features of portable chest X-ray accurately classifies COVID-19 lung infection," *BioMedical Engineering Online*, vol. 19, no. 1, pp. 88–18, 2020.

[14] A. P. Rodrigues, R. Fernandes, A. Aakash et al., "Real-Time twitter spam detection and sentiment analysis using machine learning and deep learning techniques," *Computational Intelligence and Neuroscience*, vol. 2022, Article ID 5211949, 14 pages, 2022.

[15] O. Karakuş, E. E. Kuruoğlu, and M. A. Altınkaya, "Generalized Bayesian model selection for speckle on remote sensing

images," *IEEE Transactions on Image Processing*, vol. 28, no. 4, pp. 1748–1758, 2018.

[16] Y. Wu, "Combining attention-based multiple instance learning and Gaussian processes for CT hemorrhage detection," in *Proceedings of the International Conference on Medical Image Computing and Computer-Assisted Intervention*, September 2021.

[17] Y. Oh, J. C. Ye, and J. C. Ye, "Deep learning COVID-19 features on CXR using limited training data sets," *IEEE Transactions on Medical Imaging*, vol. 39, no. 8, pp. 2688–2700, 2020.

[18] S. Dash and U. Jena, "Multi-resolution Laws' Masks based texture classification," *Journal of Applied Research and Technology*, vol. 15, no. 6, pp. 571–582, 2017.

[19] J. A. Kaw, P. Bellavista, N. A. Loan, G. M. Bhat, K. Muhammad, V. H. C. De Albuquerque, "Efficient security and authentication for edge-based internet of medical things," *IEEE Internet of Things Journal*, vol. 8, no. 21, pp. 15652–15662, 2021.

[20] M. Sharma and S. Singh, "Evaluation of texture methods for image analysis," in *Proceedings of the 7th Australian and New Zealand Intelligent Information Systems Conference*, November 2001.

[21] G. T. Reddy, M. P. K. Reddy, K. Lakshmanna, and D. S. Rajput, R. Kaluri, G. Srivastava, Hybrid genetic algorithm and a fuzzy logic classifier for heart disease diagnosis," *Evolutionary Intelligence*, vol. 13, no. 2, pp. 185–196, 2020.

[22] C.-M. Wu, Y.-C. Chen, and K.-S. Hsieh, "Texture features for classification of ultrasonic liver images," *IEEE Transactions on Medical Imaging*, vol. 11, no. 2, pp. 141–152, 1992.

[23] F. Bianconi and A. Fernández, F. Smeraldi, G. Pascoletti, Colour and texture descriptors for visual recognition: a historical overview," *Journal of Imaging*, vol. 7, no. 11, p. 245, 2021.

[24] R. Kaluri, D. S. Rajput, Q. Xin et al., "Roughsets-based approach for predicting battery life in IoT," 2021, https://arxiv.org/abs/2102.06026, Article ID 06026.

[25] M. P. K. Reddy, K. Lakshmanna, R. Kaluri, D. S. Rajput, G. Srivastava, T. Baker, "Analysis of dimensionality reduction techniques on big data," *IEEE Access*, vol. 8, pp. 54776–54788, 2020.

[26] K. Kamal and R. Qayyum, S. Mathavan, T. Zafar, "Wood defects classification using laws texture energy measures and supervised learning approach," *Advanced Engineering Informatics*, vol. 34, pp. 125–135, 2017.

[27] P. Ganasala and A. D. Prasad, "Medical image fusion based on laws of texture energy measures in stationary wavelet transform domain," *International Journal of Imaging Systems and Technology*, vol. 30, no. 3, pp. 544–557, 2020.

[28] M. Latha and K.. Kavitha, "Segmentation and texture analysis of structural biomarkers using neighborhood-clustering-based level set in MRI of the schizophrenic brain," *Magnetic Resonance Materials in Physics, Biology and Medicine*, vol. 31, no. 4, pp. 483–499, 2018.

[29] R. Kumar, R. Srivastava, and S. Srivastava, "Detection and classification of cancer from microscopic biopsy images using clinically significant and biologically interpretable features," *Journal of medical engineering*, Article ID 2015, 2015.

[30] K. Lakshmanna and N. Khare, "Constraint-based measures for DNA sequence mining using Group Search optimization algorithm," *International Journal of Intelligent Engineering and Systems*, vol. 9, no. 3, pp. 91–100, 2016.

[31] V. G. V. Mahesh, C. Chen, and V. Rajangam, "Shape and texture aware facial expression recognition using spatial pyramid Zernike moments and Law's textures feature set," *IEEE Access*, vol. 9, pp. 52509–52522, 2021.

[32] C. M. J. M. Dourado, S. P. P. da Silva, R. V. M. da Nobrega, P. P. Reboucas Filho, K. Muhammad, and V. H. C. de Albuquerque, "An open IoHT-based deep learning framework for online medical image recognition," *IEEE Journal on Selected Areas in Communications*, vol. 39, no. 2, pp. 541–548, 2021.

[33] R. K. Krishnamurthy, S. Radhakrishnan, and M. Kattuva, "Particle swarm optimization-based liver disorder ultrasound image classification using multi-level and multi-domain features," *International Journal of Imaging Systems and Technology*, vol. 31, no. 3, pp. 1366–1385, 2021.

[34] N. Ohata, G. M. Bezerra, J. V. S. D. Chagas et al., "Automatic detection of COVID-19 infection using chest X-ray images through transfer learning," *IEEE/CAA Journal of Automatica Sinica*, vol. 8, no. 1, pp. 239–248, 2021.

[35] J. N. Hasoon, A. H. Fadel, R. S. Hameed et al., "COVID-19 anomaly detection and classification method based on supervised machine learning of chest X-ray images," *Results in Physics*, vol. 31, Article ID 105045, 2021.

[36] A. P. Susaiyah, S. Parvaze Pathan, and R. Swaminathan, "Classification of indirect immunofluorescence images using thresholded local binary count features," *Current Directions in Biomedical Engineering*, vol. 2, pp. 479–482, 2016.

[37] P. S. Parvaze and S. Ramakrishnan, "Extraction of multiple cellular objects in HEp-2 images using LS segmentation," *IEIE Transactions on Smart Processing & Computing*, vol. 6, no. 6, pp. 401–408, 2017.

[38] S. S. Suganthi and S. Ramakrishnan, "Anisotropic diffusion filter based edge enhancement for segmentation of breast thermogram using level sets," *Biomedical Signal Processing and Control*, vol. 10, pp. 128–136, 2014.

[39] K. Lakshmanna and N. Khare, "Mining DNA sequence patterns with constraints using hybridization of firefly and Group Search optimization," *Journal of Intelligent Systems*, vol. 27, no. 3, pp. 349–362, 2018.

[40] A. K. Ramaniharan, S. Manoharan, and R. Swaminathan, "Laplace Beltrami eigen value based classification of normal and Alzheimer MR Images using parametric and non-parametric classifiers," *Expert Systems with Applications*, vol. 59, pp. 208–216, 2016.

[41] S. Bhattacharya, P. K. Reddy Maddikunta, Q. V. Pham et al., "Deep learning and medical image processing for coronavirus (COVID-19) pandemic: a survey," *Sustainable Cities and Society*, vol. 65, Article ID 102589, 2021.

[42] K. Saleem, M. Saleem, R. Zeeshan et al., "Situation-aware BDI reasoning to detect early symptoms of covid 19 using smartwatch" IEEE sensors," *Journal*, vol. 1-1, 2022.

[43] S. M. Basha, A. V. Lira Neto, M. José Wally, S. A. Chelloug, M. A. Elaziz, and V. H. C. De Albuquerque, "Evaluation of weighted nuclear norm minimization algorithm for ultrasound image denoising," *Wireless Communications and Mobile Computing*, vol. 2022, Article ID 3167717, 13 pages, 2022.

[44] S. M. Basha and B. C. Jinaga, "Robust denoising technique for ultrasound images based on weighted nuclear norm minimization," in *Proceedings of the International Conference on Innovative Computing and Communications Advances in Intelligent Systems and Computing*, vol. 1087, October 2020.

[45] S. M. Basha and B. C. Jinaga, "A robust approach for qualitative compression in JPEG 2000 standard," in *Proceedings of the 2012 Asia Pacific Conference on Postgraduate Research in*

Microelectronics and Electronics, pp. 224–228, Hyderabad, India, December 2012.

[46] S. M. Basha and B. C. Jinaga, "A novel response dependent image compression algorithm to reduce the nonlinear effects in color images using JPEG," in *Proceedings of the 2010 IEEE Region 8 International Conference on Computational Technologies in Electrical and Electronics Engineering (SIBIRCON)*, pp. 122–125, Irkutsk, Russia, July 2010.

[47] T. R. Gadekallu, N. Khare, S. Bhattacharya, S. Singh, and K. R. Maddikunta, I.-H. Ra, M. Alazab, "Early detection of diabetic retinopathy using PCA-firefly based deep learning model," *Electronics*, vol. 9, no. 2, p. 274, 2020.

[48] T. R. Gadekallu, N. Khare, S. Bhattacharya, and P. K. Reddy, "Deep neural networks to predict diabetic retinopathy," *Journal of Ambient Intelligence and Humanized Computing*, 2020.

[49] M. Ahsan, J. Haider, and M. Kowalski4, "COVID-19 detection from chest X-ray images using feature fusion and deep learning," *Sensors*, vol. 21, no. 4, p. 1480, 2021.

[50] D. N. Le, V. S. Parvathy, D. Gupta, A. Khanna, J. J. P. C. Rodrigues, and K. Shankar, "IoT enabled depthwise separable convolution neural network with deep support vector machine for COVID-19 diagnosis and classification," *International Journal of Machine Learning and Cybernetics*, vol. 12, no. 11, pp. 3235–3248, 2021.

[51] N.. Otsu, "A threshold selection method from gray-level histograms," *IEEE transactions on systems, man, and cybernetics*, vol. 9, no. 1, pp. 62–66, 1979.

[52] W.. Sweldens, "Lifting scheme: a new philosophy in biorthogonal wavelet constructions," in *Proceedings of the Wavelet applications in signal and image processing III*, vol. 2569, International Society for Optics and Photonics, San Diego, CA, USA, July 1995.

[53] K. El Asnaoui, Y. C. Chawki, and I. Idri, "Automated methods for detection and classification pneumonia based on x-ray images using deep learning," *Artificial Intelligence and Blockchain for Future Cybersecurity Applications*, Springer, Berlin, Germany, pp. 257–284, 2021.

[54] Y. Oh, S. Park, and J. Ye, "Deep learning covid-19 features on cxr using limited training data sets," *IEEE Transactions on Medical Imaging*, vol. 39, no. 8, pp. 2688–2700, 2020.

[55] A. I. Khan, J. Latief Shah, and M. MudasirBhat, "CoroNet: a deep neural network for detection and diagnosis of COVID-19 from chest x-ray images," *Computer Methods and Programs in Biomedicine*, vol. 196, 2020.

[56] E. Hemdan, E. Din, A. S. Marwa, and M. E. Karar, "Covidx-net: a framework of deep learning classifiers to diagnose covid-19 in x-ray images," 2020, https://arxiv.org/abs/2003.11055, Article ID 11055.

[57] B. Sekeroglu and I. Ozsahin, "Detection of COVID-19 from chest X-ray images using convolutional neural networks," *SLAS Technology*, vol. 25, no. 6, pp. 553–565, 2020.

[58] M. Pal, "Random forest classifier for remote sensing classification," *International Journal of Remote Sensing*, vol. 26, no. 1, pp. 217–222, 2005.

[59] C.-Yu Chang, S. Bhattacharya, P. M. Raj Vincent, K. Lakshmanna, and K. Srinivasan, "An efficient classification of neonates cry using extreme gradient boosting-assisted grouped-support-vector network," *Journal of Healthcare Engineering*, vol. 2021, Article ID 7517313, 14 pages, 2021.

[60] Y. Wu, A. Schmidt, E. Hernández-Sánchez, R. Molina, and A. K. Katsaggelos, "Combining attention-based multiple instance learning and Gaussian processes for CT hemorrhage detection," in *Proceedings of the International Conference onMedical Image Computing and Computer Assisted Intervention – MICCAI 2021*, Strasbourg, France, September 2021.

[61] E. E. Kuruoglu and Y. Li, "Modelling time-varying epidemiological parameters for COVID-19," *Ercim News*, vol. 124, pp. 25-26, 2021.

[62] M. B. Rodrigues, R. V. M. Da Nobrega, S. S. A. Alves et al., "Health of things algorithms for malignancy level classification of lung nodules," *IEEE Access*, vol. 6, pp. 18592–18601, 2018.

[63] P. Soda, N. C. D. Amico, J. Tessadori, and G. Valbusa, "AIforCOVID: predicting the clinical outcomes in patients with COVID-19 applying AI to chest-X-rays. an Italian multicentre study," *Medical Image Analysis*, vol. 74, Article ID 102216, 2021.

[64] A. Cohen, I. Daubechies, and J. -C. Feauveau, "Biorthogonal bases of compactly supported wavelets," *Communications on Pure and Applied Mathematics*, vol. 45, no. 5, pp. 485–560, 1992.

[65] M. Sokolova and L. Lapalme, "A systematic analysis of performance measures for classification tasks," *Information Processing & Management*, vol. 45, no. 4, pp. 427–437, 2009.